Hysteretic effects and magnetotransport of electrically switched CuMnAs

Jan Zubáč,[1,2,*] Zdeněk Kašpar,[1,2] Filip Krizek,[1] Tobias Förster,[3] Richard P. Campion,[4] Vít Novák,[1] Tomáš Jungwirth,[1,4] and Kamil Olejník[1,†]

[1]*Institute of Physics, Czech Academy of Sciences, Cukrovarnická 10, 162 00 Prague 6, Czech Republic*
[2]*Faculty of Mathematics and Physics, Charles University, Ke Karlovu 3, 121 16 Prague 2, Czech Republic*
[3]*Hochfeld-Magnetlabor Dresden (HLD-EMFL) and Würzburg-Dresden Cluster of Excellence ct.qmat, Helmholtz-Zentrum Dresden-Rossendorf, 01328 Dresden, Germany*
[4]*School of Physics and Astronomy, University of Nottingham, Nottingham NG7 2RD, United Kingdom*

(Received 15 July 2021; accepted 20 October 2021; published 19 November 2021)

Antiferromagnetic spintronics allows us to explore storing and processing information in magnetic crystals with vanishing magnetization. In this paper, we investigate magnetoresistance effects in antiferromagnetic CuMnAs upon switching into high-resistive states using electrical pulses. By employing magnetic field sweeps up to 14 T and magnetic field pulses up to ∼60 T, we reveal hysteretic phenomena and changes in the magnetoresistance, as well as the resilience of the switching signal in CuMnAs to the high magnetic field. These properties of the switched state are discussed in the context of recent studies of antiferromagnetic textures in CuMnAs.

DOI: 10.1103/PhysRevB.104.184424

I. INTRODUCTION

Antiferromagnetic materials have attracted attention in contemporary spintronics due to their unique features: The fast terahertz magnetization dynamics of antiferromagnets overcomes the gigahertz limit of their ferromagnetic counterparts used in present-day microelectronics (e.g., in magnetic random-access memories). Zero net magnetization due to the alternating magnetic moments on neighboring atoms and the resulting absence of stray fields are advantageous for memory applications requiring high integration density with no cross-talk among adjacent devices [1,2]. On the other hand, antiferromagnets have low sensitivity to external magnetic fields. This limits the implementation of schemes used for the manipulation of magnetic moments in ferromagnets and has, until recently, hindered research into practical applications of antiferromagnetic materials.

One of the possible methods to control the antiferromagnetic order is based on Néel spin-orbit torques, which were predicted in materials with specific symmetries. For example, an efficient Néel vector reorientation can be generated by a fieldlike spin-orbit torque when the antiferromagnetically coupled magnetic atoms occupy inversion-partner lattice sites [3]. A tetragonal collinear antiferromagnet CuMnAs with Néel temperature $T_N = 480$ K [4,5] is an example of a material for which this switching mechanism was experimentally demonstrated [6,7]. In this material, electrical control of the antiferromagnetic moments was also detected by the anisotropic magnetoresistance (AMR) [6]. However, the AMR-related signals were rather small, with relative resistance changes limited to tenths of a percent [6–9]. Apart from CuMnAs, the electrical control of magnetic moments was also demonstrated in Mn_2Au [10–12] and other antiferromagnetic materials [13–16].

Recently, we reported switching of CuMnAs into highly resistive states using optical or unipolar electrical pulses with the relative resistivity change reaching 20% at room temperature and approaching 100% at low temperatures [17]. After the writing pulse, the resistive signals relax following a stretched-exponential time dependence with a characteristic timescale showing a simple exponential dependence on temperature. Unlike the spin-orbit torque reorientation of the Néel vector controlled by the angle or polarity of the switching current, the unipolar switching mechanism is independent of the writing current direction and the polarization of the switching laser pulses. Complementary imaging measurements, including x-ray magnetic linear dichroism photoemission electron microscopy (XMLD-PEEM) and magneto-Seebeck microscopy [17,18], have shown that the observed large switching signals were accompanied by nanofragmentation of magnetic domains. This unipolar mechanism, which is principally distinct from the spin-orbit torque reorientation of the Néel vector, was called quench switching. In addition, recent imaging by differential-phase-contrast scanning transmission electron microscopy (DPC-STEM) [19] revealed that complex magnetic textures in CuMnAs can even include atomically sharp 180° domain walls.

The effects of the applied magnetic field on CuMnAs films and devices were previously studied [9] by means of magnetotransport measurements, XMLD spectroscopy, and XMLD-PEEM. The study demonstrated a spin-flop transition and spin reorientation at a magnetic field of ∼2 T in CuMnAs thin films with uniaxial and biaxial magnetic anisotropies, respectively. Measurements in the spin-flop (reorientation) fields confirmed that AMR associated with the reorientation of the Néel vector is on the ∼0.1% scale in CuMnAs.

*zubac@fzu.cz
†olejnik@fzu.cz

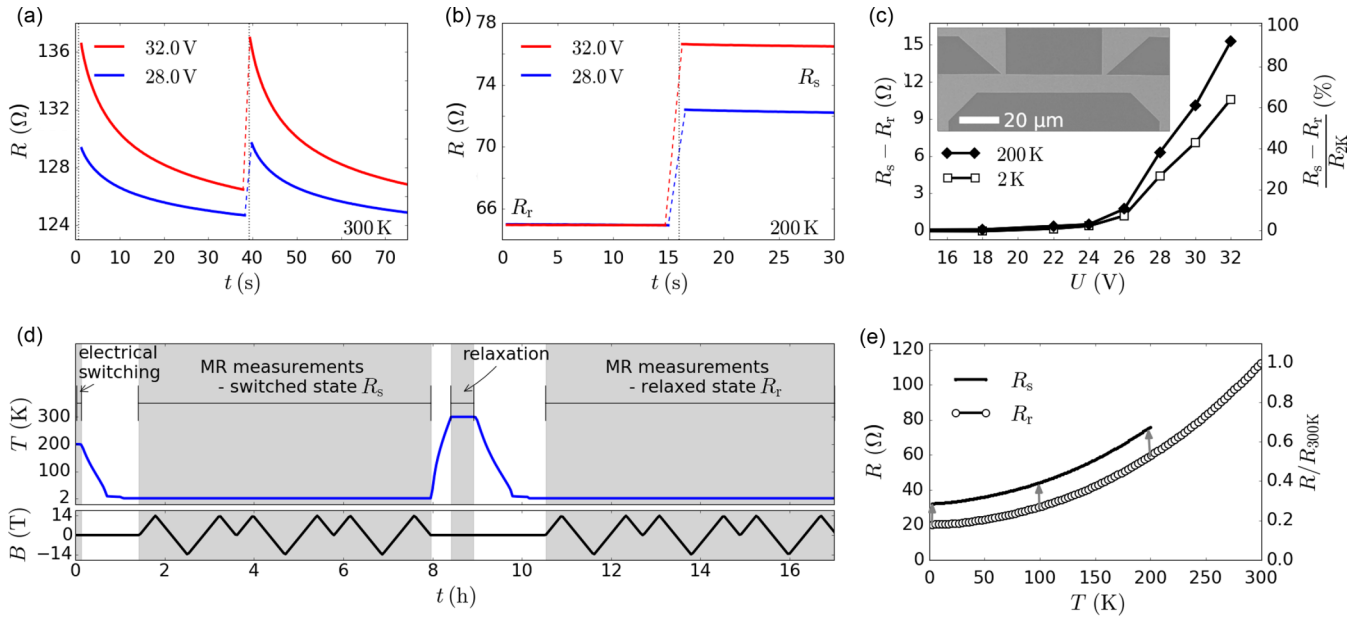

FIG. 1. (a) Electrical switching of a typical Hall bar device at 300 K showing relaxation of a signal. Single unipolar 100 μs writing pulses of two different voltage amplitudes and the longitudinal resistance readout were employed. The dotted lines mark the positions of the individual pulses. (b) Nonrelaxing resistance signal after the electrical switching from a relaxed state (R_r) to the switched state (R_s) at 200 K. (c) Magnitude of the signal induced by electrical switching at 200 K evaluated at 200 K during switching [see (b)] and at 2 K as the difference between the switched resistance and the resistance after relaxation [see (d)]. The highest pulse voltage of 32 V corresponds to a current density of $\sim 1.2\times10^7$ A/cm^2. The inset shows a scanning electron microscope micrograph of a typical Hall bar device. (d) Outline of the main experiment: After electrical switching at 200 K the sample is rapidly cooled down to a temperature of 2 K, at which MR field-sweep measurements in the quenched switched state are performed. Then the sample is warmed up and kept at a temperature of 300 K for 30 min to recover its equilibrium relaxed state. Afterwards, MR in the relaxed state at 2 K is measured in the same manner and with the same field sweep rate of 0.66 T/min as in the switched state. (e) Temperature dependence of the resistance of a typical Hall bar device measured in the relaxed state (open circles) and switched state (black line). Arrows are used to denote a shift of resistance by $\Delta R = R_s - R_r$ due to the electrical switching by 30 V pulses at 200 K. Both curves were obtained during heating for the current applied along the [$\bar{1}$00] CuMnAs direction.

In this paper, we investigate the quenched highly resistive states of CuMnAs at strong magnetic fields. Magnetoresistance (MR), i.e., the dependence of the material's resistance on the applied magnetic field, is a straightforward method to examine both magnetic and transport characteristics of metallic thin films. This phenomenon can have multiple origins, but the following should be especially taken into consideration for antiferromagnetic CuMnAs: (i) the above-mentioned AMR, (ii) ordinary metallic MR caused by the Lorentz force, (iii) the spin-disorder contribution to the resistance, and (iv) domain wall MR, which can substantially affect the device resistance in particular when containing the sharp domain walls with high densities [20].

Our paper is organized as follows: Sec. II describes the employed experimental methods. In Sec. III, we present the main results: First, we outline the scheme of the main MR experiment (Fig. 1). Then, we show the qualitative differences between the MRs of the quenched highly resistive state and the relaxed state and the correspondence between the size of the switching signal and the magnitude of the changes detected in the MR. We also address the anisotropy of the observed effects and the behavior at extreme magnetic fields. In Sec. IV, we discuss our MR results in the context of the earlier magnetic-texture microscopy studies. Finally, Sec. V summarizes our results.

II. EXPERIMENTAL METHODS

Tetragonal CuMnAs films 50 nm thick with 20 Ω sheet resistance were grown by molecular beam epitaxy on GaP(001) substrates and capped with 3 nm of Al to prevent oxidation. Characterization by atomic force and scanning electron microscopy, superconducting quantum interference device (SQUID) magnetometry, x-ray diffraction, and transport measurements showed high crystal quality and optimal electrical switching performance of the prepared samples. In particular, SQUID magnetometry data, which are typically dominated by a large negative diamagnetic signal of the GaP substrate, do not show any substantial magnetic moment after subtraction of this linear diamagnetic contribution. Further details of sample growth and characterization were recently described in Ref. [21].

Hall bars (width 10 μm, length 50 μm) used in experiments were patterned by electron beam lithography and wet etching [see the inset in Fig. 1(c) for a scanning electron microscopy image of the fabricated device].

Magnetoresistance measurements up to 14 T were performed using the electrical transport option of the physical property measurement system. The system utilizes the digital lock-in technique and is equipped with a rotator for in-plane angular scans. Selected samples were later exposed to

magnetic field pulses with a magnitude of ∼60 T and a total duration of ∼150 ms at the Dresden High Magnetic Field Laboratory. Resistance evolution during the magnetic field pulse was recorded by a high-speed digitizer; the obtained data were processed using a lock-in technique.

III. RESULTS

A. Electrical switching and the magnetotransport measurement protocol

In Figs. 1(a)–1(c) we demonstrate the switching of our CuMnAs Hall bars by unipolar electrical pulses with distinct voltage amplitudes at different base temperatures. Whereas at 300 K the resistance after the electrical pulse noticeably decays towards the initial low value [Fig. 1(a)], a high-resistance state is preserved, and negligible relaxation is observed after the pulsing at 200 K [Fig. 1(b)]. Besides this, the resistive signal scales up with the applied pulse voltage, as illustrated in Fig. 1(c) for the switching at 200 K. Our previous work [17] showed that the signal induced by the electrical switching consists of two main components with different relaxation times, τ_1 and τ_2. By examining the temporal and temperature dependencies of switching, we established that both components follow the stretched exponential function $\sim\exp[-(t/\tau_{1(2)})^{0.6}]$, and their relaxation times depend exponentially on temperature as $\tau_{1(2)} = \tau_0 \exp(E_{1(2)}/k_B T)$. The dependencies are consistent with relaxation behavior recognized in many complex systems such as glassy materials [22,23]. Using the activation energies $E_1/k_B = 9240$ K, $E_2/k_B = 7830$ K, and $1/\tau_0$ in the terahertz range from Ref. [17], we get $\tau_1 \sim 10$ s for the main switching component and $\tau_2 \sim 10$ ms for the minor fast-relaxing component at 300 K and $\tau_1 \sim 10^7$ s and $\tau_2 \sim 10^4$ s at 200 K for the two components. These expressions and parameters explain the observed nondecaying behavior after cooling and allow us to realize MR measurements in the electrically switched state with virtually infinite relaxation times at low temperatures (∼2 K).

The design of the main MR experiment is schematically presented in Fig. 1(d). At first, the electrical switching is performed at 200 K. Immediately after the switching, the sample is rapidly cooled down to 2 K, maintaining the high resistance of the switched state. After temperature stabilization, MR curves for the magnetic field applied along selected crystallographic directions are collected. To recover the low-resistance relaxed state, the sample is heated up and annealed at 300 K for 30 min ($\gg \tau_{1(2)}$). Subsequently, the sample is again cooled down to 2 K, and MR measurements are repeated in the same manner, but this time in the relaxed state.

Figure 1(e) shows the temperature dependence of the resistance measured on a typical Hall bar device in the relaxed (R_r) and switched (R_s) states. The relaxed-state resistance exhibits smoothly varying metallic behavior with a residual resistance ratio ≈6, obtained from the 300 and 2 K measurements, indicating the high crystal quality of the samples. The switched state is offset by $\delta R = R_s - R_r$. This difference does not change substantially in the displayed temperature range from 2 to 200 K.

B. Field-sweep magnetotransport up to 14 T

Figure 2 shows the main changes in the MR produced by the quench switching. Whereas the relaxed-state MR [Fig. 2(b)] displays essentially identical MRs for both up and down field sweeps, the MR in the high-resistance switched state [Fig. 2(a)] exhibits pronounced hysteretic effects. Moreover, a distinct response of the switched and relaxed states to the magnetic field is reflected in the change in the high-field slope of the MR curves. To highlight the differences between the two states, we subtracted the relaxed-state MR from the switched-state MR, and the result is presented in Fig. 2(c). The evolution of the hysteretic magnetization process and its main features are indicated by arrows and numbers: (1.) First, the resistance follows the virgin curve during the magnetic field increase. (2.) Second, we record a higher resistance trace from 14 to 0 T and a subsequent drop in the resistance to a lower value after crossing the zero-field point and continuing to −14 T. The MR curve (3.) is then recorded when the field is swept from −14 to 14 T to complete a butterfly-shaped pattern. Subsequent magnetic field sweeps in the range from −14 to 14 T can be described by repeating curves of types 2 and 3 with the crossing at the same remanent resistance in the zero field. No considerable erasing of the overall switching signal by the magnetic field can be identified. The MR traces show reproducible hysteretic behavior with a maximum width of the hysteresis at approximately 4 T. Additional measurements of minor hysteresis loops in the switched state of CuMnAs are presented in Fig. S1 in the Supplemental Material [24].

To demonstrate the close connection between the electrical switching and the changes observed in the MR, we repeated the magnetotransport measurements for several magnitudes of the switching signal. The obtained difference MR data are presented in Fig. 3(a). For small switching signals ($\lesssim$20%), the switched-state MR roughly follows its relaxed-state counterpart, giving an almost constant difference MR curve. For larger switching signals, we observe sizable hysteresis accompanied by a change in the high-field slope [Figs. 3(b) and 3(c)]. These two effects are the dominant features emerging in the MR after the switching. Qualitatively similar but quantitatively varying effects were also observed for different mutual current and field configurations (see Supplemental Figs. S2 and S3 for details [24]).

In Fig. 4, we explore the anisotropy of the switching-induced changes by measuring the longitudinal resistance during magnetic field rotations. The experimental procedure used here was analogous to that of field-sweep measurements. In tetragonal systems with competing uniaxial and biaxial anisotropies, the longitudinal AMR can be described by the following expression [25]:

$$\Delta R/\overline{R} = C_I \cos(2\psi) + C_U \cos(2\phi) + C_C \cos(4\phi) + C_{IC} \cos(4\phi - 2\psi), \quad (1)$$

where ψ is the angle between the Néel vector and the probing current j, ϕ is the angle between the Néel vector and the [100] crystalline direction of CuMnAs, and the individual terms represent the noncrystalline AMR contribution C_I, the uniaxial (C_U) and cubic (C_C) crystalline contributions, and the mixed crystalline and noncrystalline contribution C_{IC}.

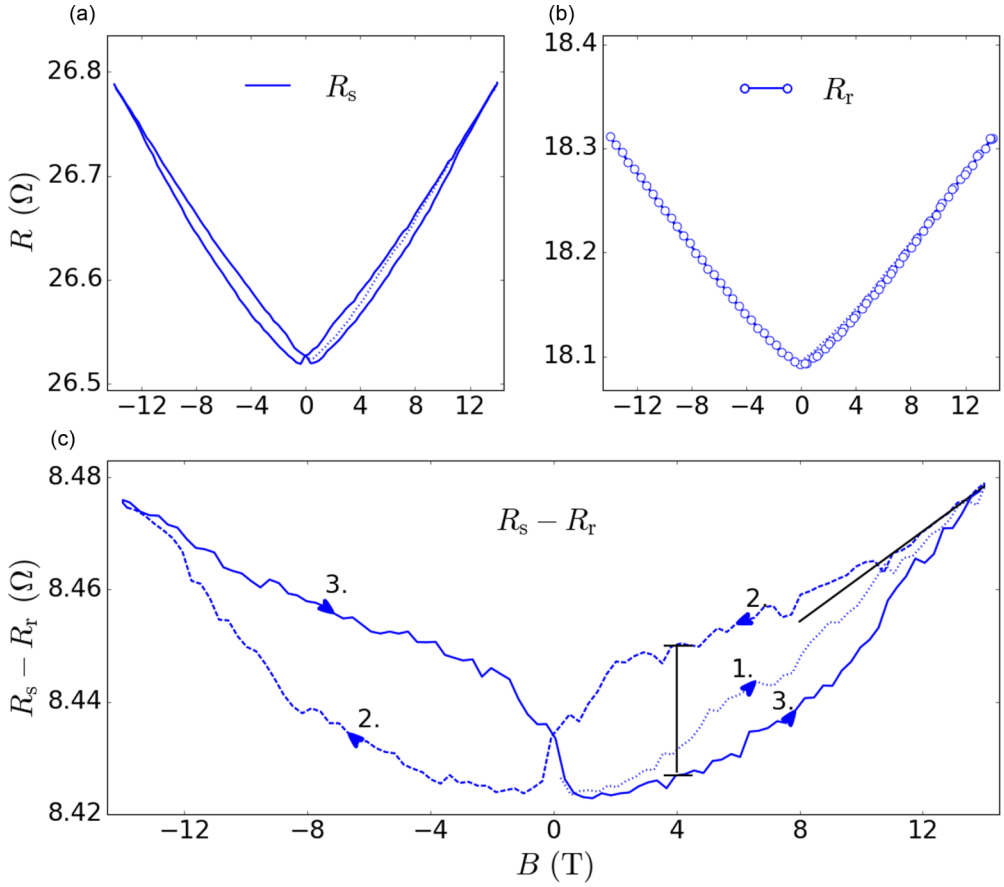

FIG. 2. Magnetoresistance of CuMnAs at 2 K (a) in the high-resistance switched state R_s for a switching signal ∼8.5 Ω and (b) in the low-resistance relaxed state R_r. The data were collected for the $j \parallel B \parallel [\bar{1}00]$ configuration. The dotted line represents the first sweep up after cooling the sample. (c) Difference $R_s - R_r$ between the switched-state and relaxed-state magnetoresistances, showing the main effects induced by the quench switching: significant hysteretic behavior and a change in the high-field slope. Black lines mark the hysteresis magnitude at 4 T and the slope from the linear fit of the sweep down in the range 10–14 T. Arrows and numbers indicate the development of the hysteretic magnetization process. Further discussion is given in the text.

For both $j \parallel [\bar{1}00]$ and $j \parallel [010]$ in the switched and relaxed states [Fig. 4(a)], the observed AMR shows the presence of twofold and fourfold terms, as expected from Fig. 1, with a relatively larger strength of fourfold crystalline terms at higher fields, consistent with the relaxed-state MR (Supplemental Fig. S4) and the AMR measurements of 50 nm thick films in Ref. [9]. (For a detailed Fourier analysis of the relaxed-state and switched-state data, see Supplemental Material Figs. S5 and S6 [24]) However, whereas the switched-state data follow approximately the same dependence as the relaxed data at low fields, they depart and go out of phase at higher fields. Despite the higher-order AMR contributions being present in both curves, the difference between the switched and relaxed states reduces to a simple $A\cos(2\psi)$ form, as shown in Fig. 4(b). This uniaxial contribution produced by switching is for both $j \parallel [\bar{1}00]$ and $j \parallel [010]$ oriented along the current (and Hall bar) direction; that is, it is a term with the same symmetry as the twofold noncrystalline AMR contribution in Fig. 1. In Fig. 4(c) we summarize the angle-dependent resistance measurements by plotting the amplitude of the difference between the switched and relaxed states as a function of the magnetic field strength. We note that the data show a nearly linear scaling with the field and a change in sign for $j \parallel [010]$. This change indicates the presence of several competing MR effects with a distinct field dependence.

C. Pulsed-field magnetoresistance up to ∼60 T

Next, we study magnetotransport of CuMnAs at extremely high magnetic fields at which we exposed the samples to magnetic field pulses up to ∼60 T. The earlier work in Ref. [9] reported magnetoresistances of 10 nm thick CuMnAs films at magnetic fields up to 30 T. They showed a behavior typical of uniaxial systems with a spin-flop transition at ≈2 T and smoothly varying MR at high fields.

Recently, magnetoresistance effects on the order of ∼1% were observed in antiferromagnetic Mn_2Au at low temperatures and at fields up to 60 T [26]. A transient abrupt change in MR in Mn_2Au observed above ≃30 T in both easy and hard field directions was attributed to removing the domain walls by forced reorientation of the magnetic moments and the associated reduction of the domain wall contribution to the total resistance. Moreover, a persistent field-induced AMR contribution to MR on the order of ∼0.1% was also recorded

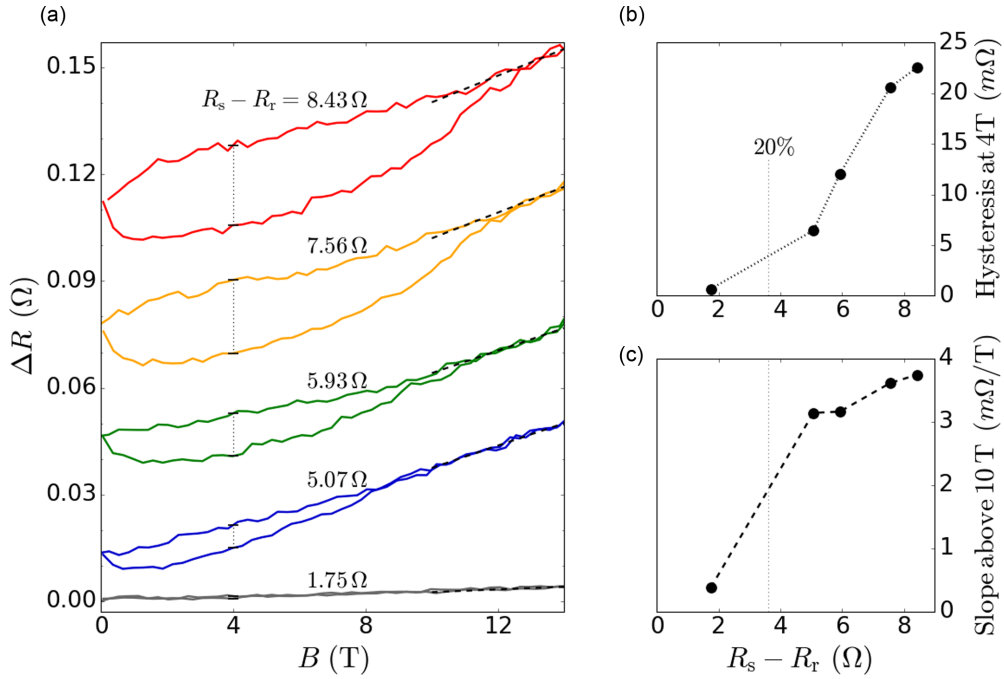

FIG. 3. (a) Difference MR curves between the switched and relaxed states for various switching signal magnitudes. The data were taken for the $j \parallel B \parallel [\bar{1}00]$ configuration; the virgin MR curve is not shown. Individual dependencies were further shifted by an arbitrary value for clarity. (b) Development of the hysteresis size and (c) the high-field slope with the switching signal size for the data in (a). The switching signal $(R_s - R_r)/R_{2K} = 20\%$ is indicated by a gray vertical line.

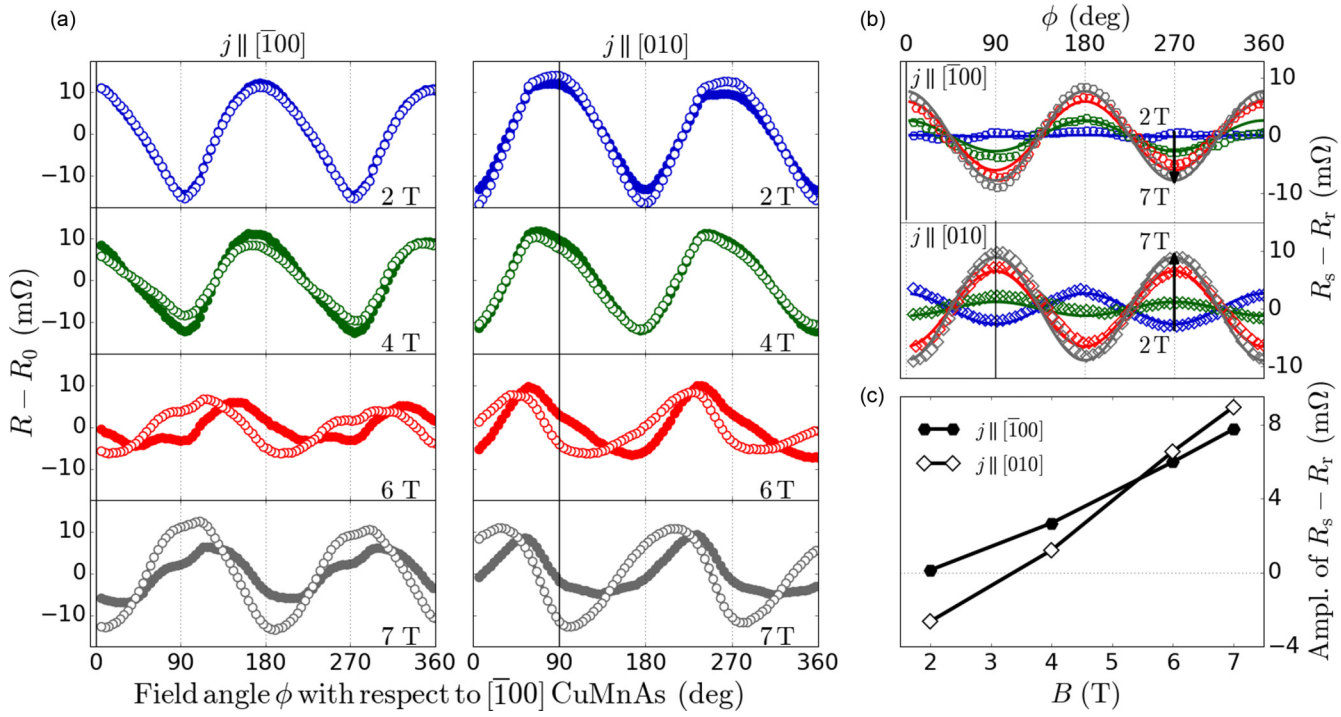

FIG. 4. (a) Resistance at 2 K during magnetic field rotations at various field strengths for the $j \parallel [\bar{1}00]$ and $j \parallel [010]$ current directions. Solid symbols represent the MR data in the switched state after the 30 V electrical pulse at 200 K; open symbols show the MR in the relaxed state. Solid vertical lines indicate the current direction. The individual angular scans were collected at increasing fields from 2 to 7 T; the data for the field rotation from 0° to 360° coincided with those taken during rotation from 360° back to 0° (not shown). (b) Difference between the switched and relaxed MR data for increasing field strengths. The solid lines represent fits to the $A\cos(2\psi)$ function. (c) The amplitude of differential resistance as obtained by fitting to the $A\cos(2\psi)$ function in (b).

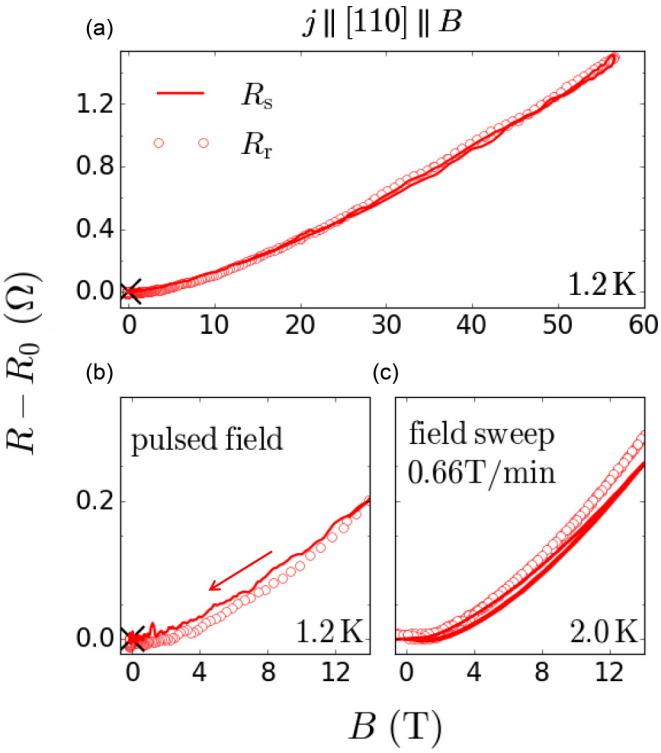

FIG. 5. (a) Magnetoresistance of CuMnAs in the pulsed magnetic field at low temperature. The switched-state MR R_s for a switching signal of 7.2 Ω is plotted by a solid line; open symbols show the MR in the relaxed state R_r. Data from the sweep up below 10 T had to be omitted due to the large noisy pickup signal (typical for the given type of measurement). The resistance R_0 in the switched state at zero field immediately before the magnetic field pulse is highlighted by the black cross. (b) Detail of the pulsed-field MR from (a) below 14 T. (c) MR data obtained at a field sweep rate of 0.66 T/min without switching (open symbols) and after electrical switching with a signal magnitude of 6.8 Ω (solid line).

in this material. These findings were supported by subsequent XMLD-PEEM imaging of the magnetic structure, which showed a reorientation of the Néel vector to the direction perpendicular to the field and a corresponding redistribution of magnetic domains and their sizes when exposed to high magnetic fields [27].

In Fig. 5, we present the high-field pulsed magnetoresistance measurements of CuMnAs in the relaxed state (without prior switching) and in the switched state. In both cases, the high-field data show a smooth variation with overlapping MRs for both increasing and decreasing fields. Also, the same zero-field resistance is measured before and after the magnetic field pulse. This suggests that the erasing of magnetic domain walls analogous to that in Mn_2Au is not possible in either the relaxed or switched state of CuMnAs and that the observed high-field MR evolution is related to a continuous spin reorientation within domains and other ordinary MR effects, in agreement with Ref. [9]. Moreover, the hysteretic behavior observed at the lower quasistationary fields (Fig. 3) is not promoted further by the ∼60 T field pulses, implying that the fields below 14 T are already sufficient for the saturation of the hysteresis [see Figs. 5(b) and 5(c) for a comparison of the corresponding low-field data after comparable switching]. Additional temperature-dependent relaxed-state MR data at pulsed fields with various orientations (Supplemental Fig. S7 [24]) display the largest overall MR change (∼8%) at ∼2 K. At higher temperatures, the relative magnitude of MR drops, and no abrupt magnetoresistive changes are detected.

IV. DISCUSSION

In this paper, we have studied the magnetotransport of CuMnAs in the quench-switched and relaxed states. Let us now focus on the two main findings of our measurements. First, the quenched highly resistive state exhibits pronounced hysteretic effects and changes in slope in the magnetoresistance (Fig. 3). Second, the increase of the resistance of the switched state cannot be removed by the magnetic field even when the field reaches 60 T (Fig. 5). In the following paragraphs, we discuss these results in the context of the recently published microscopy [19] and transport [17] measurements.

We start from the observation that the large magnetic fields do not significantly alter the increase in the resistance induced by the quench switching. Previous XMLD-PEEM and magnetoresistance measurements [9] showed that the magnetic field can reorient the Néel vector and drive 90° domain walls in CuMnAs. In contrast, our study of the quench switching signal shows that this mechanism is insensitive to fields that are significantly larger than the Néel vector reorientation (domain wall motion) fields. Furthermore, recent DPC-STEM measurements revealed additional antiferromagnetic textures in CuMnAs in the form of atomically sharp 180° domain walls [19]. Combining these results with our high-field MR measurements, we surmise that these sharp domain walls could be responsible for the high resistance of the quench-switched state. With the spin reversal occurring abruptly between two neighboring magnetic sites, the atomically sharp 180° domain walls are distinct from the 90° (or 180°) domain walls observed in XMLD-PEEM measurements whose width is approximately 100 nm. Since the two domains separated by the atomically sharp 180° domain wall have antiparallel Néel vectors, they are rotated coherently by the magnetic field, leaving the sharp 180° domain wall unaffected. In other words, the atomically sharp 180° domain walls cannot be manipulated by the spin reorientation mechanism [28]. On the other hand, they can readily explain the large and field-insensitive quench-switching resistive signal.

Within the picture of the coexisting wide and atomically sharp domain walls, we can also explain the observed hysteresis of MR in the quench-switched state. We consider the intertwined atomically sharp domain walls to influence the Néel vector reorientation and the motion of the wide domain walls. Atomically sharp domain walls at densities high enough to generate sizable resistive switching signals can serve as pinning centers for the wide 90° domain walls and hinder their motion. Correspondingly, the magnitude of the hysteretic MR reaches ∼0.1%, consistent with the observed AMR scale in CuMnAs [9]. At lower densities of the sharp domain walls (and corresponding lower quench-switching signals $\lesssim 20\%$), this effect is less pronounced, and the MR is only slightly modified compared to the relaxed state.

V. SUMMARY

In summary, we reported hysteretic phenomena and slope changes in the magnetoresistance of CuMnAs when the sample is quench switched into highly resistive states by electrical pulses. The magnitude of the effects scales up with the increasing resistive quench-switching signal. We also observed that, apart from the weak and transient MR effects, the highly resistive quench-switched state cannot be erased by a magnetic field as high as 60 T. We interpreted the observed MR phenomena in terms of the interplay of wide 90° domain walls and atomically sharp 180° domain walls, reported earlier in XMLD-PEEM and DPC-STEM imaging experiments in CuMnAs.

ACKNOWLEDGMENTS

This work was supported by Ministry of Education of the Czech Republic Grants No. LNSM-LNSpin and No. LM2018140, Czech Science Foundation Grant No. 21-28876J, and EU FET Open RIA Grant No. 766566. Experiments at magnetic fields up to 14 T were performed at MGML, which is supported within the program of Czech Research Infrastructures (Project No. LM2018096). For the pulsed-field measurements, we acknowledge the support of the HLD at HZDR, a member of the European Magnetic Field Laboratory (EMFL). We also acknowledge fruitful discussions with K. Výborný during the preparation of the paper.

[1] T. Jungwirth, X. Marti, P. Wadley, and J. Wunderlich, Nat. Nanotechnol. **11**, 231 (2016).
[2] V. Baltz, A. Manchon, M. Tsoi, T. Moriyama, T. Ono, and Y. Tserkovnyak, Rev. Mod. Phys. **90**, 015005 (2018).
[3] J. Železný, H. Gao, K. Výborný, J. Zemen, J. Mašek, A. Manchon, J. Wunderlich, J. Sinova, and T. Jungwirth, Phys. Rev. Lett. **113**, 157201 (2014).
[4] P. Wadley *et al.*, Nat. Commun. **4**, 2322 (2013).
[5] P. Wadley, V. Hills, M. R. Shahedkhah, K. W. Edmonds, R. P. Campion, V. Novák, B. Ouladdiaf, D. Khalyavin, S. Langridge, V. Saidl, P. Nemec, A. W. Rushforth, B. L. Gallagher, S. S. Dhesi, F. Maccherozzi, J. Železný, and T. Jungwirth, Sci. Rep. **5**, 17079 (2015).
[6] P. Wadley *et al.*, Science **351**, 587 (2016).
[7] P. Wadley, S. Reimers, M. J. Grzybowski, C. Andrews, M. Wang, J. S. Chauhan, B. L. Gallagher, R. P. Campion, K. W. Edmonds, S. S. Dhesi, F. Maccherozzi, V. Novak, J. Wunderlich, and T. Jungwirth, Nat. Nanotechnol. **13**, 362 (2018).
[8] J. Volný, D. Wagenknecht, J. Železný, P. Harcuba, E. Duverger-Nedellec, R. H. Colman, J. Kudrnovský, I. Turek, K. Uhlířová, and K. Výborný, Phys. Rev. Mater. **4**, 064403 (2020).
[9] M. Wang *et al.*, Phys. Rev. B **101**, 094429 (2020).
[10] S. Y. Bodnar, L. Šmejkal, I. Turek, T. Jungwirth, O. Gomonay, J. Sinova, A. Sapozhnik, H.-J. Elmers, M. Kläui, and M. Jourdan, Nat. Commun. **9**, 348 (2018).
[11] S. Yu. Bodnar, M. Filianina, S. P. Bommanaboyena, T. Forrest, F. Maccherozzi, A. A. Sapozhnik, Y. Skourski, M. Kläui, and M. Jourdan, Phys. Rev. B **99**, 140409(R) (2019).
[12] M. Meinert, D. Graulich, and T. Matalla-Wagner, Phys. Rev. Appl. **9**, 064040 (2018).
[13] N. L. Nair, E. Maniv, C. John, S. Doyle, J. Orenstein, and J. G. Analytis, Nat. Mater. **19**, 153 (2020).
[14] Y. Cheng, S. Yu, M. Zhu, J. Hwang, and F. Yang, Phys. Rev. Lett. **124**, 027202 (2020).
[15] L. Baldrati, O. Gomonay, A. Ross, M. Filianina, R. Lebrun, R. Ramos, C. Leveille, F. Fuhrmann, T. R. Forrest, F. Maccherozzi, S. Valencia, F. Kronast, E. Saitoh, J. Sinova, and M. Kläui, Phys. Rev. Lett. **123**, 177201 (2019).
[16] M. Dunz, T. Matalla-Wagner, and M. Meinert, Phys. Rev. Res. **2**, 013347 (2020).
[17] Z. Kašpar, M. Surýnek, J. Zubáč, F. Krizek, V. Novák, R. P. Campion, M. S. Wörnle, P. Gambardella, X. Marti, P. Němec, K. W. Edmonds, S. Reimers, O. J. Amin, F. Maccherozzi, S. S. Dhesi, P. Wadley, J. Wunderlich, K. Olejník, and T. Jungwirth, Nat. Electron. **4**, 30 (2021).
[18] T. Janda *et al.*, Phys. Rev. Mater. **4**, 094413 (2020).
[19] F. Krizek, S. Reimers, Z. Kašpar, A. Marmodoro, J. Michalička, O. Man, A. Edstrom, O. J. Amin, K. W. Edmonds, R. P. Campion, F. Maccherozzi, S. S. Dnes, J. Zubáč, J. Železný, K. Výborný, K. Olejník, V. Novák, J. Rusz, J. C. Idrobo, P. Wadley, and T. Jungwirth, arXiv:2012.00894.
[20] A. D. Kent, J. Yu, U. Rüdiger, and S. S. P. Parkin, J. Phys.: Condens. Matter **13**, R461 (2001).
[21] F. Krizek, Z. Kašpar, A. Vetushka, D. Kriegner, E. M. Fiordaliso, J. Michalicka, O. Man, J. Zubáč, M. Brajer, V. A. Hills, K. W. Edmonds, P. Wadley, R. P. Campion, K. Olejník, T. Jungwirth, and V. Novák, Phys. Rev. Mater. **4**, 014409 (2020).
[22] V. S. Dotsenko, M. Feigel'man, and L. Ioffe, *Spin Glasses and Related Problems* (CRC Press, Boca Raton, FL, 1991), Vol. 1.
[23] T. Lookman and X. Ren, *Frustrated Materials and Ferroic Glasses*, Springer Series in Materials Science Vol. 275 (Springer, Berlin, Heidelberg, 2018).
[24] See Supplemental Material at http://link.aps.org/supplemental/10.1103/PhysRevB.104.184424 for supporting measurements and figures.
[25] A. W. Rushforth, K. Výborný, C. S. King, K. W. Edmonds, R. P. Campion, C. T. Foxon, J. Wunderlich, A. C. Irvine, P. Vašek, V. Novák, K. Olejník, J. Sinova, T. Jungwirth, and B. L. Gallagher, Phys. Rev. Lett. **99**, 147207 (2007).
[26] S. Y. Bodnar, Y. Skourski, O. Gomonay, J. Sinova, M. Kläui, and M. Jourdan, Phys. Rev. Appl. **14**, 014004 (2020).
[27] A. A. Sapozhnik, M. Filianina, S. Y. Bodnar, A. Lamirand, M.-A. Mawass, Y. Skourski, H.-J. Elmers, H. Zabel, M. Kläui, and M. Jourdan, Phys. Rev. B **97**, 134429 (2018).
[28] O. Gomonay, T. Jungwirth, and J. Sinova, Phys. Rev. Lett. **117**, 017202 (2016).